J. Phys. Chem. **1989,** *93,* 8059–8067

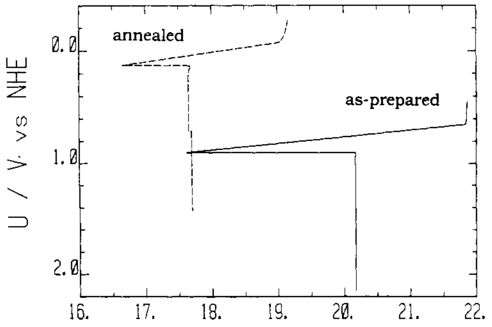

Figure 8. Density of states functions for the as-prepared and additionally annealed iron–titanium oxide electrodes that were used to calculate the simulated curves in Figure 7.

potential, which is equivalent to the energy scale. There are two important differences between the density of states functions. One effect of the annealing treatment is that the density of states above the flatband potential is reduced by more than a factor of 500. Second, the flatband potential of the annealed sample is over 0.5 V more negative than of the as-prepared sample. The decrease in the density of localized states which is a result of the annealing process is associated with the corresponding crystallization of the oxide. Interestingly, the concentration of states in the annealed sample remains constant in the band gap, at least to energies approximately 1.5 eV below the bulk Fermi level. The presence of these states in the more ordered oxide indicates that transition-metal oxide possess complex electronic structures that are not completely described by the simple band model used for elemental semiconductors, such as silicon or germanium. For example, oxygen vacancies and excess cations can exist in a material that has a high degree of structural order and these defects may result in localized electronic states outside the principal bands. Also, the shift in the flatband potential, which corresponds to a shift in the bulk Fermi level, shows that a major redistribution of the electrons occurred because of the annealing process. The decrease in the density of localized states at lower energies due to the crystallization of the sample and perhaps changes in stoichiometry may force the electrons to occupy states at higher energies thereby raising E_F, or equivalently, making U_{fb} more negative.

Conclusions

An equation for the charge density was derived as a function of potential for continuous distributions of localized states. A generaly equation for the capacity was used to perform model calculations for an n-type semiconductor using exponentially decaying density of states functions as well as constant bands of localized states with varying widths. Combinations of these two types of functions were also investigated.

Results show that Mott–Schottky plots that are curved in certain potential ranges are obtained, with the specific shape depending on the density of states function used.

Linear Mott–Schottky behavior is found in potential ranges where the concentration of states at energies less than $E_F - e\Delta\phi_{sc}$ is negligible. However, linearity in a C^{-2} vs potential plot does not necessary indicate the validity of the Mott–Schottky equation.

Capacity data for an amorphous iron–titanium oxide electrode were fitted by using the model. Data obtained after the annealing treatment were also fitted, and significant differences in the density of states functions before and after annealing were found.

Acknowledgment. This work was supported in part by the National Science Foundation and Columbia University.

Registry No. Iron titanium oxide, 12789-64-9.

Adsorbate-Enhanced Chemisorption in the CO/Re(001) System: Experiment and Theory

O. M. Becker, I. Chacham, M. Asscher, and A. Ben-Shaul*

Department of Physical Chemistry and The Fritz Haber Molecular Dynamics Research Center, The Hebrew University of Jerusalem, Jerusalem 91904, Israel

(Received: January 4, 1989; In Final Form: May 5, 1989)

The chemisorption kinetics of CO molecules on Re(001) crystal surface was studied by temperature-programmed desorption (TPD) experiments in the crystal temperature range of 80–360 K. Correlation was found between the population of the tightly bound, partially dissociated, β-CO state and the less tightly bound α-CO state; basically, the α-state starts to populate when the β-sites approach saturation. Furthermore, the increase in β-CO coverage is accompanied by an increase in the overall sticking probability, as well as in the nonmonotonic coverage dependence of the peak desorption temperature of the α-state. The chemisorption kinetics was found to be crystal temperature independent. LEED analysis reveals that the CO overlayer is disordered, as reported previously. A theoretical model is proposed to account for the above observations. In this model, the β-sites are treated as traps for mobile α-CO admolecules. Occupied β-sites then serve as nucleation centers for enhanced, extrinsic precursor-mediated, chemisorption and island growth. The nonmonotonic variation of α-CO adsorption energy, and the appearance of a shoulder in the α-CO TPD peak at high coverages, are explained by a lattice gas model, incorporating repulsive nearest-neighbor and attractive next-nearest-neighbor lateral interactions between the chemisorbed molecules.

1. Introduction

The concept of a weakly bound (physisorbed) precursor state is often employed in the analysis of adsorption and desorption experiments. As demonstrated by Kisliuk over 30 years ago,[1] the formation of an ("extrinsic") mobile precursor[2] initially trapped above occupied lattice sites can explain why chemisorption probabilities are often larger than the values predicted by Langmuir's classical model. In some systems, the sticking coefficient, $S(\theta)$, not only exceeds the Langmuirian behavior ($S(\theta) = S_0(1-\theta)$, θ = coverage) but actually goes through a maximum

---

(1) (a) Kisliuk, P. *Phys. Chem. Solids* **1957**, *3*, 95. (b) Kisliuk, P. *Phys. Chem. Solids* **1958**, *5*, 78. See also, e.g.: Tompkins, F. C. *Chemisorption of Gases on Metals*; Academic Press: London, 1978.

(2) Cassuto, A.; King, D. A. *Surf. Sci.* **1981**, *102*, 388.

at intermediate θ. This unusual behavior of $S(\theta)$ has been observed for example in the O_2/W(110),[3] N_2/Ru(001),[4] and recently also in the O_2/Pt(111) system.[5,6]

The initial increase of $S(\theta)$ with θ in the N_2/Ru(001) system has been attributed by Menzel et al.[4] to a special interplay involving lateral interactions between two adsorption states of the N_2 molecules, corresponding to two peaks in the temperature-programmed desorption (TPD) spectrum. An alternative explanation was given by Hood et al.,[7] who emphasize the dominant role of precursor-mediated chemisorption adsorbate–adsorbate interactions, and antiphase domain boundaries. On the basis of Monte Carlo simulations, these authors argue that the origin of the rise of $S(\theta)$ at low coverages is the (weak but multiple) attractive interactions between extrinsic precursor molecules trapped above *islands* of chemisorbed molecules and the underlying layer. Adsorbate lateral interactions can also lead to increased chemisorption probability at island boundaries. In fact, enhanced sticking probability at the circumference of the islands formed during chemisorption suffices (i.e., without invoking the formation of a precursor state) to explain the increase of $S(\theta)$ at low θ. This has been suggested by Steininger et al.[6] as the mechanism governing $S(\theta)$ in the O_2/Pt(111) system. Yet, another possibility to explain the behavior of this system is based on an extended Kisliuk model in which the adsorption probability of the extrinsic precursor is higher than that of an isolated molecule, as suggested by Winkler et al.[5] General adsorption models incorporating the effects of direct chemisorption, precursor states, island growth, lateral interactions, and diffusion vs desorption rates are discussed elsewhere.[8-13] The effect of lateral interactions on other aspects of the adsorbate–metal bond such as vibrational frequencies, work function, etc., are discusssed for example in ref 14–16.

In this paper, we present a combined experimental and theoretical study of the CO/Re(001) system. The major experimental characteristics of this system, as reflected by the TPD spectra, are the appearance of two distinct adsorption sites and, as in the systems described above, a sticking coefficient $S(\theta)$, exhibiting an increase with θ at low coverages. These features resemble somewhat the behavior observed by Menzel et al. in the N_2/Ru(001).[4] However, while in this system the two states correspond to rather low and similar chemisorption binding energies (~6 and ~7 kcal/mol, the difference being attributed to lateral interactions), in the CO/Re(001) system, the difference in binding energy is ~20 kcal/mol (~45 kcal/mol for the strongly bound β-state and ~25 kcal/mol for the α-state), reflecting the different binding of a molecular α-state and a partially dissociated β-state.[17,18]

Following the analysis of the experimental results in section 3, we present in section 4 a rather simple theoretical model capable of explaining the principal kinetic, structural, and energetic features characterizing the CO/Re system. A basic assumption of the model is that the strongly binding β-sites behave initially as traps for mobile α-CO molecules. Once populated, these sites become nucleation centers for enhanced, precursor-mediated, chemisorption and island growth. In addition, due to lateral interactions, the already chemisorbed molecules can enhance (or inhibit, depending on coverage) chemisorption into neighboring vacant sites. Fine details of the TPD spectra are explained in terms of a lattice gas model, involving repulsive nearest-neighbor (NN) and attractive next-nearest-neighbor (NNN) lateral interactions between the chemisorbed CO molecules.

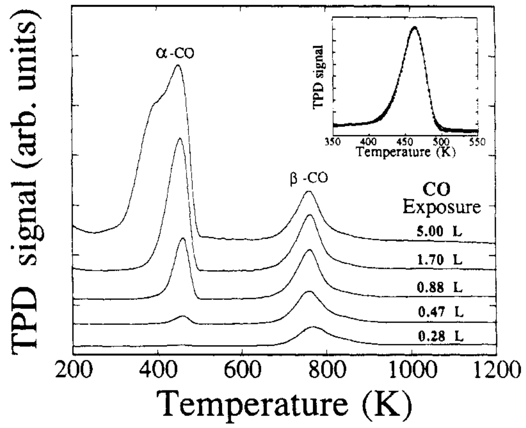

Figure 1. TPD spectra of CO from Re(001) at 200 K. The α-CO and β-CO states are indicated above the desorption peaks at 460 and 780 K, respectively. The inset demonstrates a typical TPD line-shape analysis simulation (full line) of a low-coverage α-CO desorption (open squares) at a heating rate (B) of 12.3 K/s. The coverage-dependent desorption rate constant parameters are as follows: $k_d = \nu \exp[-(E_\alpha^0 + b\theta_\alpha)/kT]$, $\nu = 10^{11}$ s^{-1}, $E_\alpha^0 = 23$ kcal/mol, and $b = 5$ kcal/mol at $\theta_\alpha = 0.07$.

2. Experimental Section

The experiments described here were performed in an ultra-high-vacuum (UHV) stainless steel chamber, with a base pressure of 3×10^{-10} mbar as described elsewhere.[19,20] The cleaning procedure of the Re(001) sample involves Ar^+ sputtering at 1000 V (12-μA sample current) for 4 min, then at 500 V for 1 min, and followed by an annealing at 1500 K for 3 min. Auger analysis, using a CLAM-100 VG spectrometer, reveals a less than 3% oxygen and carbon contamination level. The sample holder is connected to a pair of copper feedthroughs, attached at the bottom of a liquid nitrogen dewar that is mounted on top of a differentially pumped, rotary flange. The sample is attached to the copper feedthrough via two W–Re alloy wires of 0.12-mm diameter, on both sides of the crystal. The sample temperature was monitored by a pair of W–5% Re vs W–26% Re thermocouple wires spot welded to the edge of the sample. By means of a microprocessor control, we could get any temperature in the range 80–1800 K, using an ac-current resistive heating procedure, at an accuracy level of ±0.5 K, or linear heating ramps at rates of 0.5 K/s up to 50 K/s. A typical cooling time from 1800 to 80 K is 6 min.

The experimental results described here are based on TPD measurements carried out using a quadrupole mass spectrometer (QMS) (VG SX-200) attached to the UHV chamber via a translation stage. It is shielded by a conical tube; the circular edge of it is 1 mm from the sample when fully extended. The aperture of this shield allows a line of sight with a 0.12-cm^2 area at the center of the sample, thus minimizing contributions to the TPD signal from the holder and edges of the sample. The data from the QMS are digitized and stored by the same microprocessor that controls the sample temperature. Each data point (see Figure 1, inset) is the average of four measurements, taken during the TPD runs. The stored data are then transferred to a minicomputer for a TPD line-shape analysis by means of a numerical integration

---

(3) Wang, C.; Gomer, R. *Surf. Sci.* **1979**, *84*, 329.

(4) Feulner, P.; Menzel, D. *Phys. Rev. B* **1982**, *25*, 4295.

(5) Winkler, A.; Guo, X.; Siddiqui, H. R.; Hagans, P. L.; Yates, J. T., Jr. *Surf. Sci.* **1988**, *201*, 419.

(6) Steininger, H.; Lehwald, S.; Ibach, H. *Surf. Sci.* **1982**, *123*, 1.

(7) Hood, E. S.; Toby, B. H.; Weinberg, W. H. *Phys. Rev. Lett.* **1985**, *55*, 2437.

(8) Pfnür, H.; Menzel, D. *J. Chem. Phys.* **1983**, *79*, 2400.

(9) Pfnür, H.; Feulner, P.; Menzel, D. *J. Chem. Phys.* **1983**, *79*, 4613.

(10) Evans, J. W.; Nord, R. S.; Rabaey, J. A. *Phys. Rev. B* **1988**, *37*, 8589.

(11) Becker, O. M.; Ben-Shaul, A. *Phys. Rev. Lett.* **1988**, *61*, 2859.

(12) Silverberg, M.; Ben-Shaul, A.; Rebentrost, F. *J. Chem. Phys.* **1985**, *83*, 6501.

(13) Silverberg, M.; Ben-Shaul, A. *J. Chem. Phys.* **1987**, *87*, 3178; *J. Stat. Phys.* **1988**, *52*, 1179; *Surf. Sci.*, in press.

(14) Hesket, D.; Plummer, E. W.; DePaola, R. A.; Eberhardt, W.; Hoffmann, F. M.; Moser, H. R. *Surf. Sci.* **1985**, *164*, 490.

(15) Brubaker, M. E.; Trenary, M. *J. Chem. Phys.* **1986**, *85*, 6100.

(16) DePaola, R. A.; Hoffmann, F. M.; Hesket, D.; Plummer, E. W. *Phys. Rev. B* **1987**, *35*, 4236.

(17) (a) Ducros, R.; Tardy, B.; Bertolini, J. C. *Surf. Sci.* **1983**, *128*, L219. (b) Ducros, R.; Fusy, J.; Jupille, J.; Tatarenko, S. *Appl. Surf. Sci.* **1987**, *29*, 179.

(18) Gasser, R. P. H.; Holt, D. E. *Surf. Sci.* **1977**, *64*, 520.

(19) Haase, G.; Asscher, M. *Surf. Sci.* **1987**, *191*, 75.

(20) Peled, H.; Asscher, M. *Surf. Sci.* **1987**, *183*, 201.

(21) Chacham, I.; Asscher, M. Unpublished results.

(22) Marchon, B.; Ogletree, D. F.; Salmeron, M.; Siekhous, W. *J. Vac. Sci. Technol.* **1988**, *A6*(2), 531.

(23) Deckert, A. A.; Brand, J. L.; Arena, M. V.; George, S. M. *J. Vac. Sci. Technol.* **1988**, *A6*(3), Part I, 288.

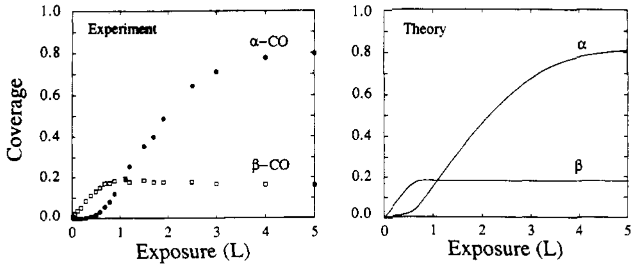

Figure 2. CO uptake from the α-state and the β-state as a function of CO gas exposure at crystal temperature of 200 K experiment (left) and theory (right) (see text).

of the desorption rate equation[19] and for total uptake measurements.

The sample is a slice of 0.5 cm^2 cut from a 99.99% pure Re single-crystal rod, oriented to better than 1° of the (001) direction by X-ray Laue back-reflection, then polished on both sides by diamond paste down to a 0.25-μm grain.

The CO gas was 99.8% pure (Air Products) and was used without further purification.

3. Results

The TPD spectra of CO desorbing from Re(001), following several different initial exposures at a sample temperature of 200 K, are shown in Figure 1. Very similar spectra characterize the system at all adsorption temperatures between 80 and 360 K. In Figure 1, we see that for exposures below 0.25 langmuir (1 langmuir = 10^{-6} Torr·s), only the more tightly bound, presumably partially dissociated β-CO, state is populated. (For a detailed discussion of the binding and spectral characteristics of the β-CO state on Re(001), see ref 17 and 18). The α-state begins to appreciably populate only when the exposure reaches ~0.8 langmuir, at which point the β-state becomes essentially saturated. This behavior is more clearly demonstrated in Figure 2, which displays the separate α- and β-populations as a function of CO exposure, at a crystal temperature of 200 K. From the analysis of the coverage vs exposure curve (Figure 2), it follows that the β-state saturates at $\theta = \bar{\theta}_\beta \simeq 0.18\theta_s$ (corresponding to an exposure of 0.8 langmuir), with θ_s denoting the saturation CO coverage. Hereafter, we set $\theta_s = 1$; i.e., all coverages are given relative to the saturation value.

The inset of Figure 1 describes a line-shape analysis of the α-CO peak, corresponding to an initial α-CO coverage of $\theta_\alpha = 0.07$. In this analysis, an Arrhenius-type first-order desorption rate, $-\mathrm{d}\theta_\alpha/\mathrm{d}T = -(\mathrm{d}\theta_\alpha/\mathrm{d}t)/B = (\theta_\alpha/B)\nu \exp[-E_\alpha(\theta_\alpha)/kT]$, is used to fit the experimental results, with $B = \mathrm{d}T/\mathrm{d}t = 12.3$ K/s denoting the linear rate of the temperature sweep. Parametrization of $E_\alpha(\theta_\alpha)$ was obtained with $E_\alpha(\theta_\alpha) = E_\alpha^0 + b\theta_\alpha$; the following parameters have yielded the best fit: $\nu = 10^{11\pm1}$ s^{-1}, $b = 5$ kcal/mol, and $E_\alpha^0 = 23.0 \pm 0.5$ kcal/mol. E_α^0 is the limiting (zero-coverage) binding energy of an α-CO molecule. In section 4, we shall consider in more detail the θ dependence of $E_\alpha(\theta)$ and in section 5 discuss the physical meaning of the parameter b.

The α-CO and β-CO adsorption isotherms shown in Figure 2 were determined by measuring the area under the TPD peaks at 465 and 780 K for various exposures. This area was then divided by the area under the overall CO uptake (i.e., under both the 465 and the 780 K TPD peaks), following CO exposure of 20 langmuir. This exposure determines the saturation coverage. CO on Re(001) does not form an ordered overlayer,[20,24] and only a diffused (1 × 1) pattern is observed at any CO coverage. Therefore, the absolute number of CO molecules per squared-centimeters at saturation coverage, N_s, is difficult to determine. The estimate in the literature[17] is $N_s = 6 \times 10^{14}$ cm^{-2}, corresponding to a saturation coverage of CO/Re(001) equal to 0.4. The uncertainty associated with this value is unknown, especially because of the unknown distribution and character of the defects on the surface. In Figure 3, the total CO uptake ($\alpha + \beta$ states) vs exposure is shown for three different adsorption temperatures. (The CO gas temperature is constant at 295 K throughout the experiments presented here.) It is seen that in the crystal temperature range of 80–360 K the sticking probabilities into either the α- or the β-states are nearly independent of temperature, regardless of coverage. The inset in Figure 3 magnifies the data points for very low exposures at crystal temperature of 200 K. From the slope of the relative coverage vs exposure curve at $\theta \rightarrow 0$, we get the initial sticking probability, S_0. It is derived from the general expression

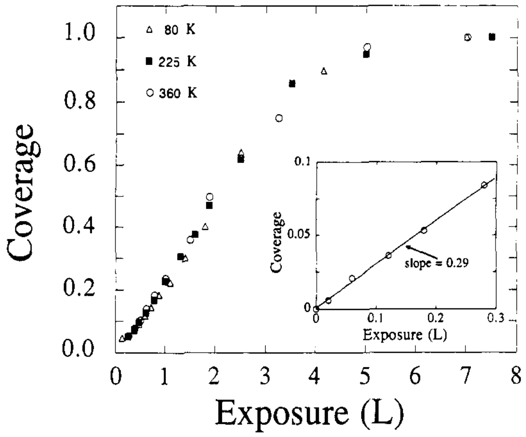

Figure 3. Total CO uptake, both α-CO and β-CO, as a function of CO exposure at three crystal temperatures: 80 K (open triangle), 225 K (filled square), and 360 K (open circle). The inset shows the data points as $\theta \rightarrow 0$ at crystal temperature of 200 K.

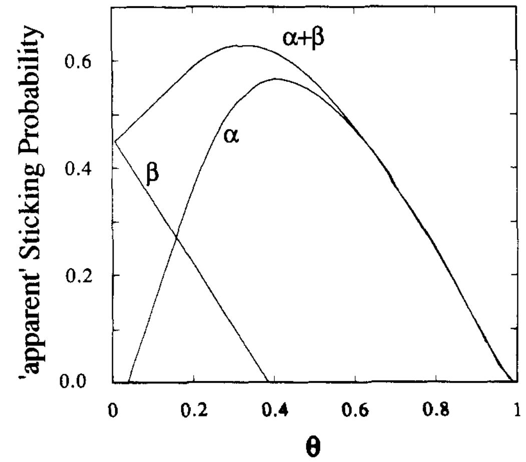

Figure 4. "Apparent" sticking probability of CO into the β-state, the α-state, and the overall sticking probability ($\alpha + \beta$) as a function of the total CO coverage at crystal temperature of 200 K (experimental results).

$$N_s(\mathrm{d}\theta/\mathrm{d}\epsilon) = (2\pi MkT)^{-1/2}S(\theta)$$

where M is the molecular mass, k is the Boltzmann constant, and T is the gas temperature. As shown in the inset in Figure 3, $\mathrm{d}\theta/\mathrm{d}\epsilon = 0.29$ at $\theta \rightarrow 0$, implying $S_0 = S(\theta \rightarrow 0) = 0.45 \pm 0.1$. This value is obtained for exposures $\epsilon \leq 0.3$ langmuir and for several adsorption temperatures in the range 80–360 K. It should be noted that the ± 0.1 uncertainty in S_0 reflects the error associated with the slope of the θ vs ϵ curves (over the entire temperature range). It does not account for the uncertainties related to the value of N_s.

Using the equation above, we obtain $S(\theta) = S_{\alpha+\beta}(\theta)$ from the (normalized) slope of $\mathrm{d}\theta/\mathrm{d}\epsilon \propto \mathrm{d}\theta/\mathrm{d}t$. The result is shown in Figure 4. $S(\theta)$ is approximately 0.45 at $\theta = 0$, and it then increases to ~0.6 near $\theta \approx 0.35$, from which point it decreases monotonically with coverage down to zero at saturation. Similar procedures were applied to analyze the θ_α and θ_β curves in Figure 2. The corresponding contributions to S are described by curves α and β in Figure 4. Note that while $\mathrm{d}\theta/\mathrm{d}t = \mathrm{d}(\theta_\alpha + \theta_\beta)/\mathrm{d}t$ is proportional to the total sticking probability $S(\theta)$, the separate contributions

---

[24] Doodley, G. J.; Haas, T. W. *Surf. Sci.* **1970**, *19*, 1.

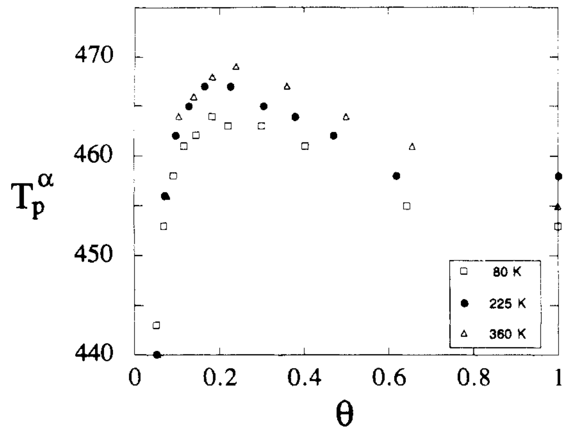

Figure 5. Peak desorption temperature of the α-CO state (T_p^α) as a function of the initial total CO coverage for three crystal temperatures.

$d\theta_i/dt$ ($i = \alpha,\beta$) cannot be simply interpreted as (being proportional to) sticking probabilities. This is because CO molecules can diffuse from α- to β-sites (and, in principle, also in the opposite direction) in the course of the adsorption process and similarly so during the desorption experiments that we use to determine θ_α and θ_β. (The derivatives $d\theta_i/dt$ may be regarded as "apparent" sticking probabilities.) Further discussion of the adsorption process is given in sections 4 and 5.

The thermal desorption peak temperature of the α-CO state is shown in Figure 5 as a function of initial coverage. It is seen that at very low coverage ($\theta \leq 0.08$), $T_p^\alpha = 441 \pm 4$ K, and then it goes through a maximum of 465 ± 3 K at coverages near 0.3 and drops to about 455 ± 3 K for coverages approaching saturation. This variation of T_p^α with θ is insensitive to the crystal temperature during adsorption. An interpretation of this behavior in terms of adsorbate lateral interactions is given in the next two sections.

4. Discussion and Model

The major qualitative conclusions relevant for understanding the kinetic, energetic, and structural characteristics of the CO/Re(001) system may be summarized by the following experimental findings: (a) the appearance of two distinct TPD peaks, i.e., the α- and β-states at ~465 and 780 K, respectively; (b) the lack of a LEED pattern other than the substrate's hexagonal (1 × 1) structure at any overlayer coverage; (c) the "nonstandard" coverage dependence of the sticking coefficient, as reflected by the rise of $S(\theta)$ with θ at low coverages, Figure 4; (d) the minor influence of the initial adsorption temperature (in the range 80–360 K) on the total coverage and thus on the sticking probability, Figure 3, and on the desorption kinetics, as reflected by the TPD spectra, Figures 1 and 5; and (e) the nonmonotonic change of T_p^α with coverage, Figure 5.

Our aim in this section is to formulate a simple model that can rationalize, or at least be consistent with, the above experimental finding, using as few assumptions and unknown parameters as possible.

The peak of the α-state in the TPD spectrum at $T_p^\alpha \approx 465$ K corresponds to a typical CO–metal binding energy, ~25 kcal/mol. On the other hand, the β-peak at $T_p^\beta \approx 780$ K indicates a very tightly bound CO molecule (~45 kcal/mol). The large difference between the binding energies, ~20 kcal/mol, strongly suggests that the α- and β-states correspond to different types of adsorption sites. Isotope scrambling measurements indicate that the β-sites involve a partially dissociated state of the CO molecules.[18] The strongly binding β-sites may be located at steps, dislocations, or other defects on the densely packed Re(001) surface.[17] It is therefore very likely that the β-sites appear in small *clusters*, randomly distributed on the surface, a picture consistent with additional findings, as noted below.

In order to check this hypothesis, we increased the defects density on the surface by sputtering without annealing. The TPD spectra of CO following the adsorption on the sputtered surface have shown that the β-CO population increased by more than a factor of two relative to the α-CO population.[21] In addition, a recent scanning tunneling microscopy study[22] indicates that the defects on the annealed Re(001) surface (which shows a rather clear hexagonal LEED pattern) seem to appear in clusters with large terraces between them.

The analysis of the TPD spectra (see Figures 1 and 2) reveals very clearly that as long as the total coverage is lower than the saturation coverage of β-sites ($\theta < \bar{\theta}_\beta \simeq 0.18$), the desorbing CO molecules come out mainly from β-sites. This behavior implies that the (strongly binding) β-sites are, in fact, "traps", capturing diffusing α-CO molecules, from which they escape only at very high temperatures ($T \simeq 780$ K) directly into the gas phase. On the basis of the TPD spectra alone, it is not obvious whether the preferential population and saturation (at $\theta < \bar{\theta}_\beta$) of the β-state is taking place already at the adsorption stage (i.e., at a relatively low temperature) or only upon heating during the TPD temperature ramp. On the basis of diffusion measurements of CO molecules adsorbed on various metals (with binding energies similar to that of α-CO on Re), one can safely assume that, at 360 K, the highest adsorption temperature in our experiments, the α-CO molecules are freely diffusing on the surface.[23] Consequently, their trapping into β-sites and the corresponding saturation of these sites is, most likely, taking place already at the adsorption stage. The negligible dependence of the results, especially of the total coverage (Figure 3), on surface temperature suggests significant α-CO mobility and a similar adsorption mechanism at lower temperatures as well.

The increase of $S(\theta)$ with θ at low coverages (Figure 4) indicates that the already chemisorbed molecules enhance the trapping and consequently the chemisorption probability of additional molecules from the gas phase. Since the first molecules adsorbed preferentially occupy β-sites, the enhanced trapping probability should be mainly attributed to β-molecules. Consistent with this notion is the fact that $S(\theta)$ reaches a maximum somewhat above $\theta \simeq \bar{\theta}_\beta$, i.e., when most of the β-sites become populated, as shown in Figure 4. These observations suggest that CO molecules from the gas phase are effectively trapped above occupied chemisorption sites, from which they find their way via lateral diffusion in the second layer until arriving at a vacant site. This, of course, is the familiar extrinsic precursor mechanism that has been previously invoked by various authors to explain "nonstandard" adsorption isotherms and $S(\theta)$ curves.[1,5–10] In particular, it has been shown that a possible reason for $S(\theta)$ to exhibit a maximum at intermediate θ is that the trapping probability on top of occupied sites, S_1, exceeds the corresponding probability above vacant sites, S_0. One explanation for such behavior was given by Gomer et al. for the O_2/W(110) system.[3] There, the occupied sites enhanced momentum transfer from the gas molecule to the surface, thus leaving the molecule with insufficient vertical momentum to allow reflection to the gas phase, resulting in increased sticking probability. Monte Carlo and other studies suggest that large S_1 values are associated with trapping the extrinsic precursor molecule above a cluster (or island) of occupied sites, due to the cooperative attractive interactions with the molecules underneath.[7,11] Following lateral diffusion in the second layer and adsorption at the island boundaries, the extrinsic precursor mechanism contributes to island growth.

The qualitative picture emerging from the discussion so far is that, following the population of the β-sites, they serve as adsorption (or nucleation) centers around which islands (of α-CO molecules) can grow. At low θ_α, the islands may disintegrate due to diffusion of the α-CO molecules. However, at high coverages, an ordered overlayer should form, *unless* the chemisorbed molecules are organized in many, small, ordered domains meeting at grain boundaries. Considering the high abundance of β-sites and their role as nuclei for domain growth, the formation of many small α-CO domains is the most reasonable explanation for the absence of a LEED pattern, other than the somewhat diffused substrate's (1 × 1), at any CO coverage on the Re(001) surface.

Lateral interactions between CO (or other) molecules adsorbed on densely packed surfaces, such as the Re(001), are often repulsive if the molecules occupy nearest-neighbor (NN) sites and attractive between next-nearest-neighbors (NNN) or higher order pairs, see, e.g., ref. 25. The coverage dependence of T_p^α, Figure 5, can be accounted for if the same behavior prevails in our system as well. For the sake of concreteness, let us assume that, indeed, NN interactions are repulsive and NNN ones are attractive, implying that the energetically favorable structure of the α-CO molecules is $(\sqrt{3} \times \sqrt{3})$R30°. It should be stressed however that there is no experimental evidence for this assumption in the CO/Re(001) system. On other closed-packed metal surfaces, e.g., Ru(001),[25] CO does form this structure. We assume the $(\sqrt{3} \times \sqrt{3})$R30° structure in our model for the CO/Re(001) system for convenience only.

At low θ_α, most of the desorbing α-CO molecules are isolated (i.e., have no neighbors around) and desorb at a relatively low temperature, $T_p^\alpha(\theta_\alpha{=}0) \simeq 440$ K, Figure 5. As θ_α increases, the attractive interactions drive the CO molecules to organize locally in the (assumed) $\sqrt{3} \times \sqrt{3}$ structure. The attractive lateral interactions also increase the effective desorption energy and consequently T_p^α. If the adlayer was perfect, i.e., free from domain boundary defects and the $\sqrt{3} \times \sqrt{3}$ was indeed the preferred structure, T_p^α would reach a maximum at $\theta_\alpha/(1 - \bar{\theta}_\beta) \simeq 0.33$ or $\theta = \theta' = \bar{\theta}_\beta + \theta_\alpha \simeq 0.47$. Both defects and a more open structure imply a lower value of θ'. Our data suggests $\theta' \simeq 0.3$. As θ_α increases further, repulsive lateral interactions become more prominent, due to both the appearance of domain boundaries and to population of the less favorable NN positions. These interactions reduce the effective binding energy of the α-CO molecules and cause a decrease in T_p^α. $T_p^\alpha(\theta_\alpha{\to}1)$ is higher than $T_p^\alpha(\theta_\alpha{=}0)$ because after the desorption of the molecules from unfavorable positions, the ones remaining adsorbed experience attractive interactions.

Although all our kinetic information on the CO/Re system derives from the TPD experiments, part of it (e.g., the θ vs exposure data) reflects some basic features of the adsorption process. Of course, the TPD results are indicative of the desorption mechanism. Since the adsorption and desorption processes take place at different time and temperature regimes, it is both convenient and appropriate to treat their kinetics separately, in accordance with the experimental procedure.

(*i*) *Adsorption Kinetics.* On the basis of the qualitative notions above, the time dependence of the α- and β-state populations during the adsorption stage is governed by the following rate equations

$$\frac{1}{J}\frac{\mathrm{d}\theta_\alpha}{\mathrm{d}t} = [S_{0\alpha} + W_\alpha](1 - \bar{\theta}_\beta - \theta_\alpha) - k\theta_\alpha(\bar{\theta}_\beta - \theta_\beta) \tag{1}$$

$$\frac{1}{J}\frac{\mathrm{d}\theta_\beta}{\mathrm{d}t} = [S_{0\beta} + W_\beta](\bar{\theta}_\beta - \theta_\beta) + k\theta_\alpha(\bar{\theta}_\beta - \theta_\beta) \tag{2}$$

with J denoting the flux of CO molecules onto the surface, i.e., the number of molecules impinging on a surface area corresponding to one adsorption site in unit time ($J \propto$ pressure). Thus, the sum of these two equations, which gives the (normalized) rate of change of the total coverage, $\theta = \theta_\alpha + \theta_\beta$, is the net chemisorption (sticking) probability:

$$S(\theta) = \frac{1}{J}\frac{\mathrm{d}\theta}{\mathrm{d}t} = [S_{0\alpha} + W_\alpha](1 - \bar{\theta}_\beta - \theta_\alpha) + [S_{0\beta} + W_\beta](\bar{\theta}_\beta - \theta_\beta) \tag{3}$$

In eq 1–3, $S_{0\alpha}$ denotes the direct chemisorption probability into an α-site, i.e., the probability that a CO molecule initially trapped above a vacant α-site will actually become chemisorbed there (or into a neighboring vacant site). W_α is the chemisorption probability associated with indirect (extrinsic precursor-mediated) adsorption, corresponding to the initial trapping of the gas molecule on top of an occupied (either α or β) adsorption site and migration toward a vacant site. W_α depends on θ_α and θ_β, is discussed in more detail below. Similarly, especially in systems governed by strong lateral interactions, $S_{0\alpha}$ may also depend on coverage (see below). $S_{0\beta}$ and W_β are defined in analogy to $S_{0\alpha}$ and W_α. Finally, the last terms in eq 1 and 2 represent the rate of conversion of α-CO into β-CO, following diffusion of the α-molecules and their trapping at β-sites. θ_α is proportional to the number of diffusing α-CO's, $(\bar{\theta}_\beta - \theta_\beta)$ is the concentration of vacant β-traps, and k is an effective (dimensionless) diffusion-trapping constant. Note that we ignore the reverse process, i.e., β → α. We also ignore desorption of the chemisorbed CO molecules during the adsorption stage that takes place at relatively low temperatures, (considerably below the low TPD peak).

Kisliuk's original model incorporates both the direct (or intrinsic precursor-mediated) and indirect (extrinsic precursor-mediated) adsorption pathways.[1] Extended and alternative models[3-12] have been proposed to account for unusual $S(\theta)$ curves, e.g., those exhibiting a maximum at intermediate θ values, as in the experiments reported here, see Figure 4. In an attempt to account for a similar behavior in the CO/Re system, we now present another variant of Kisliuk's model. This extended version takes into consideration the existence of two types of adsorption sites, the possibly different trapping (physisorption) probabilities on top of vacant and occupied sites and (approximately) the possible influence of adsorbate lateral interactions.

Let $T_{1\beta}$ denote the trapping probability of a molecule from the gas phase on top of an occupied β-site or a cluster of several such sites. Let q denote the probability that this (extrinsic precursor) molecule survives long enough to perform a lateral diffusion step in the second layer, prior to desorption into the gas phase; thus $(1 - q)$ is the desorption probability during the time interval separating (on the average) consecutive lateral jumps. ($q = w_l/(w_d + w_l)$ where w_l and w_d are, respectively, the rates of lateral jumps and desorption.) Assuming, in analogy to Kisliuk's model,[1] a random distribution of the chemisorbed α- and β-molecules (i.e., β-sites), the precursor molecule would reach, following a lateral jump, an occupied α-site with probability θ_α, an occupied β-site with probability θ_β, a vacant α-site with probability $1 - \bar{\theta}_\beta - \theta_\alpha$, and a vacant β-site with probability $\bar{\theta}_\beta - \theta_\beta$. Now let $\Gamma_{1\alpha}$ denote the probability that the molecule arriving at a vacant α-site will actually become chemisorbed there (rather than desorb or diffuse further). Then, the net chemisorption probability of a gas molecule into an α-site through a precursor state that has been captured above a β-site (the probability of which is $T_{1\beta}\theta_\beta$) and has performed just one lateral step is $T_{1\beta}\theta_\beta q(1 - \bar{\theta}_\beta - \theta_\alpha)\Gamma_{1\alpha}$. Similarly, the chemisorption probability following an intermediate jump above another occupied β-site (probability, $q\theta_\beta$) or α-site ($q\theta_\alpha$) before arriving at the vacant site is $T_{1\beta}\theta_\beta(q\theta_\beta + q\theta_\alpha)q(1 - \bar{\theta}_\beta - \theta_\alpha)\Gamma_{1\alpha}$. If n jumps separate the capture from the eventual chemisorption event, the probability will be $T_{1\beta}\theta_\beta q^{n+1}(\theta_\beta + \theta_\alpha)^n(1 - \bar{\theta}_\beta - \theta_\alpha)\Gamma_{1\alpha}$. Adding the analogous process originating with capture above an occupied α-site, i.e., $T_{1\alpha}\theta_\alpha$ replacing $T_{1\beta}\theta_\beta$, and summing (the geometric series $(q\theta)^n$) over all $n \geq 0$, we obtain the contribution $W_\alpha(1 - \bar{\theta}_\beta - \theta_\alpha)$ to $\mathrm{d}\theta_\alpha/\mathrm{d}t$ in eq 1. The explicit form of W_α is

$$W_\alpha = \frac{(T_{1\alpha}\theta_\alpha + T_{1\beta}\theta_\beta)q\Gamma_{1\alpha}}{1 - q\theta} \tag{4}$$

The corresponding expression for W_β is similar, with $\Gamma_{1\beta}$ replacing $\Gamma_{1\alpha}$. It should be noted that, for simplicity, it has been assumed that the migration probability, q, is independent of the type of the underlying occupied sites: i.e., $q_{\alpha\alpha} = q_{\alpha\beta} = q_{\beta\alpha} = q_{\beta\beta}$. We also neglect any additional kinetic restraints that might arise from the, possibly partially dissociative, character of the β-state.

If the α- and β-sites were identical so that $T_{1\alpha} = T_{1\beta} = T_1$, $\Gamma_{1\alpha} = \Gamma_{1\beta} = \Gamma_1$, and $S_{0\alpha} = S_{0\beta} = S_0$, substitution of W_α $(= W_\beta = W)$ from eq 4 into eq 3 would yield

$$S(\theta) = \frac{1}{J}\frac{\mathrm{d}\theta}{\mathrm{d}t} = \left(S_0 + \frac{S_1 q\theta}{1 - q\theta}\right)(1 - \theta) \tag{5}$$

with $S_1 \equiv T_1\Gamma_1$. This expression reduces further to Kisliuk's formula

---

[25] Williams, E. D.; Weinberg, W. H.; Sobrero, A. C. *J. Chem. Phys.* **1982**, *76*, 1150, and references cited therein. For a review, see: Weinberg, W. H. *Annu. Rev. Phys. Chem.* **1983**, *34*, 217.

$$S(\theta) = \frac{S_0(1-\theta)}{1-q\theta} \tag{6}$$

when $S_0 = S_1 = T_1\Gamma_1$. In this connection, recall that in general one can write $S_0 = T_0\Gamma_0$, with T_0 denoting the trapping probability (into an intrinsic precursor state) above an empty site and Γ_0 the probability of chemisorption from this state. In Kisluik's original model, it is assumed that $T_1 = T_0$ and $\Gamma_1 = \Gamma_0$.

It should be noted that throughout the derivations above we have assumed that the chemisorbed (both α and β) molecules are randomly distributed on the surface. This assumption is strictly valid only if molecular diffusion on the surface is rapid during the adsorption stage and if lateral adsorbate interactions play a minor role. Incorporation of adsorbate lateral interactions into adsorption models is quite complicated, requiring in general the introduction of various assumptions and new parameters.[3-12] Qualitatively, attractive adsorbate interactions tend to increase the trapping probability above occupied (especially clustered) sites,[7,11] implying $T_1 > T_0$, while the opposite holds for repulsive interactions. More generally, lateral interactions can modify T_1 and T_0 as well as the quantities Γ_1 and Γ_0 defined above. We shall briefly consider these effects while contrasting the model with the experimental data in section 5.

Lateral adsorbate interactions are known to play a very important role in desorption phenomena. In the analysis of TPD experiments, the effects of such interactions are often accounted for through a θ-dependent adsorption energy $E(\theta)$. In the following subsection, we propose a model for $E(\theta)$ appropriate for the CO/Re system, which will be tested against the experimental data in section 5.

(*ii*) *Desorption Kinetics*. As argued earlier, the variation of T_p^α with coverage depicted in Figure 5 is qualitatively explained by repulsive NN and attractive NNN interactions between the chemisorbed α-CO molecules. More specifically, let ϵ_r and ϵ_a denote the repulsive and attractive pair potentials, respectively. Assuming pairwise additivity of interaction energies, the effective binding energy of an α-CO molecule surrounded by n_r molecules in NN positions and n_a molecules in NNN positions is $E_\alpha^0 + n_r\epsilon_r + n_a\epsilon_a$ with E_α^0 denoting the binding energy of an isolated ($\theta \to 0$) α-CO molecule; note that we use $\epsilon_r < 0$ and $\epsilon_a > 0$. The apparent desorption energy at coverage θ_α is then approximately given by

$$E_\alpha(\theta_\alpha) = E_\alpha^0 + \langle n_r\rangle\epsilon_r + \langle n_a\rangle\epsilon_a \tag{7}$$

where $\langle n_r\rangle$ and $\langle n_a\rangle$ are the average numbers of NN and NNN molecules.

Various approximations can be employed to estimate $\langle n_r\rangle$ and $\langle n_a\rangle$ as a function of θ_α. For instance, we could assume that none of the repulsive NN positions is occupied as long as there are vacant attractive NNN sites. In this case, $\langle n_r\rangle = 0$ for all $\theta \leq \bar{\theta}$ corresponding to $\langle n_a\rangle \leq Z_a$, where Z_a is the maximal number (i.e., the coordination number) of NNN molecules. On a perfect hexagonal lattice, $Z_a = 6$ and $\bar{\theta} = {}^1/_3$. Better estimates of $\langle n_r\rangle$ (and $\langle n_a\rangle$) can be obtained with use of lattice gas models. We shall use here a simplified version of the Bethe–Peierls approximations.[13,26] To calculate $\langle n_r\rangle$ and $\langle n_a\rangle$, we focus attention on the two shells of Z_r nearest-neighbor and Z_a next-nearest-neighbor sites surrounding the "central" (i.e., the desorbing) CO molecule, see Figure 6. We treat this "colony"[13,26] of $Z_r + Z_a + 1$ sites as a small open system, in equilibrium, with the rest of the surface that serves as a reservoir of molecules with chemical potential μ. We take into consideration all the interaction potentials between the central molecule and its nearest-neighbors and next-nearest-neighbors, but, for mathematical simplicity, we ignore correlations between the positions of the neighbors. The probability of finding the Z_r and Z_a sites occupied by n_r and n_a neighbors, respectively, is then given by

$$P(n_r,n_a) = \frac{1}{\Xi}\binom{Z_r}{n_r}\binom{Z_a}{n_a}\phi_r^{\,n_r}\,\phi_a^{\,n_a}\,\lambda^{(n_r+n_a)} \tag{8}$$

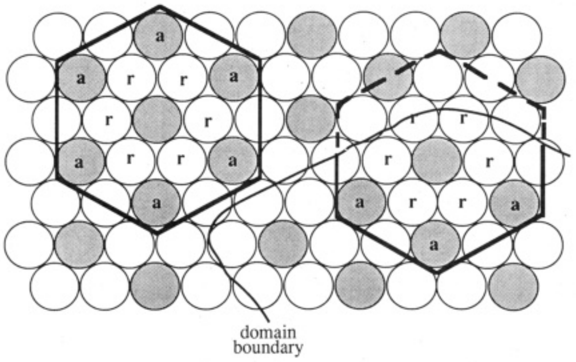

Figure 6. Schematic representation of two colonies of α-sites. The colony to the left (denoted by a hexagon) is situated in an ordered domain, hence $Z_a = Z_r$: "r" is for repulsive nearest-neighbors, and "a" is for attractive next-nearest-neighbors. The colony to the right is located by a domain boundary; the broken part of the right hexagon represents the reduced number of attractive neighbors, due to the presence of the boundary.

where $\phi_r \equiv \exp(-\epsilon_r/kT)$ and $\phi_a \equiv \exp(-\epsilon_a/kT)$, $\lambda \equiv \exp(\mu/kT)$ is the absolute activity, and Ξ is the corresponding grand canonical partition function. The activity, λ, is determined by the (particle) conservation condition

$$\begin{aligned}\langle n_r + n_a\rangle &= \sum_{n_r=0}^{Z_r}\sum_{n_a=0}^{Z_a}(n_r+n_a)\,P(n_r,n_a)\\ &= \frac{\partial \ln \Xi}{\partial \ln \lambda} = (Z_r + Z_a)\theta_\alpha\end{aligned} \tag{9}$$

Because of the simple form of $P(n_r,n_a)$, Ξ can be evaluated in closed form

$$\Xi = (1 + \lambda\phi_r)^{Z_r}\,(1 + \lambda\phi_a)^{Z_a} \tag{10}$$

which upon substitution into eq 9 yields a simple (quadratic) equation for λ involving the ϕ_i, Z_i, and θ in the coefficients. Solving for λ, we can then evaluate $\langle n_r\rangle$ and $\langle n_a\rangle$ (hence $E_\alpha(\theta_\alpha)$) using

$$\langle n_r\rangle = \frac{\partial \ln \Xi}{\partial \ln \phi_r} = \frac{\lambda\phi_r Z_r}{1+\lambda\phi_r} \tag{11}$$

with a similar expression for $\langle n_a\rangle$ in terms of $\phi_a Z_a$.

With use of eq 7 and 11 for the desorption energy, the TPD spectrum of the α-molecules can be obtained by integrating the first-order desorption rate equation

$$\frac{d\theta_\alpha}{dT} = -(\nu/B)\theta_\alpha \exp\left[-\frac{E_\alpha(\theta_\alpha)}{kT}\right] \tag{12}$$

with $B = dT/dt$ denoting the constant heating rate. For simplicity, we assume that the frequency factor, ν, in the Arrhensium rate expression is independent of coverage.

5. Model vs Experiment

The model presented in the previous section for CO adsorption on (and desorption from) the Re(001) surface involves a number of unknown parameters. The values of some of these parameters, such as the fraction of β-sites or the zero-coverage sticking probability, are uniquely dictated by the experimental data. Others can be estimated based on qualitative arguments while few are somewhat arbitrary. These considerations underlie the choice of parameters used in our calculations. Although, as we shall see below, the agreement between the model's predictions and the observed results is quite satisfactory, it should be stressed that no systematic search of parameters aiming to achieve the best fit with experiment has been attempted. Thus, we do not claim that our model is the only possible explanation of the experimental results. It is meant to be a reasonable and consistent picture of the observed behavior. As in the previous section, we discuss first

---

(26) Adams, D. L. *Surf. Sci.* **1974**, *42*, 12.

the kinetics of the adsorption process and then the kinetics of desorption.

(*i*) *Adsorption Kinetics*. From the experiment, we obtain the β-CO saturation coverage, $\bar{\theta}_\beta = 0.18$, Figure 2. From the data in Figure 3, we obtain the zero-coverage limit of the sticking probability $S_0 = S(\theta \rightarrow 0) = 0.45 \pm 0.10$. Using our eq 3 and noting that as $\theta \rightarrow 0$ (i.e., both θ_α and $\theta_\beta \rightarrow 0$) W_α and W_β vanish (see eq 4), we get

$$S_0 = S_{0\alpha}(1 - \bar{\theta}_\beta) + S_{0\beta}\bar{\theta}_\beta \qquad (13)$$

Substituting the experimental values of $\bar{\theta}_\beta$ and S_0, we obtain a relationship between $S_{0\alpha}$ and $S_{0\beta}$: $S_{0\beta} = 2.5 - 4.6S_{0\alpha}$, implying (through the requirement $0 \leq S_{0\beta} \leq 1$) $0.33 \leq S_{0\alpha} \leq 0.54$. In principle, by varying the fraction of the β-sites on the surface (i.e., by varying $\bar{\theta}_\beta$), one could obtain the specific values of $S_{0\alpha}$ and $S_{0\beta}$. At present, we do not have a simple systematic way to vary $\bar{\theta}_\beta$.

The adsorption isotherms corresponding to the α- and β-states were shown in Figure 2. The theoretical curves in this figure, which compare very well with the experimental ones, were obtained by solving eq 1 and 2 with $S_{0\alpha} = S_{0\beta}$ (=0.45) and $W_\alpha = W_\beta$, as given by eq 4. The numerical values chosen for the parameters in this expression were $T_{1\alpha} = T_{1\beta} = \Gamma_{1\alpha} = \Gamma_{1\beta} = 1$ and $q = 0.6$, for reasons explained below. It should be stressed, however, that the behavior depicted in Figure 2 is rather insensitive to these parameters. The most relevant parameter here is the dimensionless diffusion constant, k, which determines the rate of $\alpha \rightarrow \beta$ conversion and hence the "roundness" of the θ_α and θ_β curves as $\theta_\beta \rightarrow \bar{\theta}_\beta$. The theoretical curves in Figure 2 correspond to $k = 500$, which ensures fast depletion of α-CO's into the β-traps. Larger values of k will sharpen further the change in slope of the curves at $\theta_\beta = \bar{\theta}_\beta$. Similar good agreement with experiment is obtained for all k values between 100 and 1000. (Changing $S_{0\alpha}$ within the limits imposed by S_0 does not affect this conclusion significantly.) As a final remark concerning Figure 2, it should be reminded that although we regard the θ_α and θ_β curves as signatures of the adsorption process, they are actually derived from desorption data. This remark pertains mainly to the question whether CO diffusion takes place already at the adsorption stage or only later during the TPD cycle. Since activation barriers to diffusion are invariably lower than those for desorption, we can safely assume that, at least for adsorption temperatures not much below the α-CO desorption peak ($\sim$450 K), the mobility of α-CO molecules is rapid[23] and Figure 2 is an adequate picture of the adsorption process.

An alternative test of our adsorption model is provided by the total sticking coefficient, $S(\theta)$, as given by eq 3. Figure 7 shows the experimental $S(\theta)$ curve of Figure 4 and three theoretical curves, calculated on the basis of the models discussed in section 4. Recall first that an $S(\theta)$ curve exhibiting a maximum at a finite θ value is quite unusual,[3-9,11] indicating that the already chemisorbed molecules enhance further chemisorption. This behavior is in marked contrast to the simple Langmurian behavior $S(\theta) = S_0(1 - \theta)$. Similarly, Kisliuk's model,[1] as given by eq 6, although predicting a slower decrease of $S(\theta)$ with θ, cannot account for $\mathrm{d}S(\theta)/\mathrm{d}t > 0$; at most, it gives $S(\theta) = S_0 =$ constant for $q = 1$ (recall $0 \leq q \leq 1$).

The extended Kisliuk model, eq 5, can lead to the appearance of a maximum in $S(\theta)$, provided $T_1\Gamma_1 = S_1 > S_0$. Since $S_0 = 0.45$ is known experimentally, there are two unknown parameters in eq 5, S_1 and q, by the variation of which we may try to reproduce the experimental $S(\theta)$ curve. (Recall that in arriving at eq 5 a few simplifying approximations have been introduced, i.e., $S_{0\alpha} = S_{0\beta}$ and $T_{1\alpha}\Gamma_{1\alpha} = T_{1\beta}\Gamma_{1\beta}$.) It is not difficult to determine from eq 5 the coverage θ^* at which $S(\theta)$ reaches its maximum, and $S^* = S(\theta^*)$, as a function of q and S_1. Curve a in Figure 7, which corresponds to $S_1 = 1$ and $q = 0.6$, is about the best approximation for the experimental $S(\theta)$, which can be obtained with eq 5. The calculated and experimental θ^* are similar, but the calculated enhancement factor S^*/S_0, though somewhat larger than 1, is considerably lower than the experimental value, $S^*/S_0 \simeq 1.35$. Note that we have chosen the maximum possible value of $S_1 = 1$, corresponding to $T_1 = 1$ (unit trapping solubility) and $\Gamma_1 = 1$ (unit probability that an extrinsic precursor arriving above a vacant site will become chemisorbed). Then, $q = 0.6$ ensures $\theta^* \simeq \theta_{\text{exp}}^* \simeq 0.35$.

A better fit to the experimental data may be obtained by relaxing some of the assumptions embodied in eq 5. For instance, we can keep using the maximal value for S_1 (=1) but allow $S_{0\alpha} \neq S_{0\beta}$. We found that as $S_{0\beta}/S_{0\alpha}$ decreases, the calculated $S(\theta)$ better approximates the experimental one. Curve b in Figure 7 corresponds to $S_{0\beta}/S_{0\alpha} \simeq 0.1$ or, more precisely, to eq 3 with $S_{0\alpha} = 0.54$, $S_{0\beta} = 0.04$ (so that $S_0 = 0.45$), $W_\alpha = W_\beta$, $S_1 = 1$, and $q = 0.6$. Although curve b is closer to the measured $S(\theta)$, one cannot simply explain why $S_{0\beta}$ should be smaller than $S_{0\alpha}$; in fact, since β-sites are more strongly binding, the opposite behavior should be expected (unless for steric reasons the β-sites are more difficult to reach).

Except, very indirectly, through the use of $S_1 > S_0$, the models expressed by eq 4 or 5 do not account for the possible role of adsorbate lateral interactions on $S(\theta)$. In particular, if such interactions are important, the trapping probability above a vacant site (T_0) and the probability of subsequent chemisorption into this site (Γ_0) may depend on its local environment. If it is surrounded by attracting chemisorbed neighbors, $T_0\Gamma_0 = S_0$ is expected to increase and to decrease if the neighbors are repulsive. On the average, the interaction energy with the surrounding occupied sites $\epsilon(\theta)$ will be a function of the total coverage, $\epsilon(\theta) = \langle n_\mathrm{a}\rangle\epsilon_\mathrm{a} + \langle n_\mathrm{r}\rangle\epsilon_\mathrm{r}$, with $\langle n_\mathrm{a}\rangle$, ϵ_a, etc., having the same meaning as in eq 7. Consequently, it is reasonable to assume that $S_0 = T_0\Gamma_0$ varies with θ according to $S_0(\theta) = S_0(0)\ F(\epsilon(\theta))$ with F denoting a function of $\epsilon(\theta)$ (satisfying $F(\epsilon(\theta)) \rightarrow 1$ as $\theta \rightarrow 0$) and $S_0(0) = S_0(\theta{=}0) = 0.45$.

A simple, yet physically reasonable, form for F is obtained if we assume that $S(\theta)$ varies with $\epsilon(\theta)$ according to a Boltzmann (or Arrhenius-type) form, corresponding to $F(\epsilon(\theta)) = \exp(-a\epsilon(\theta)/kT)$. Curve c in Figure 7 has been obtained by integrating eq 3 with use of this form, with $\epsilon(\theta) = \langle n_\mathrm{a}\rangle\epsilon_\mathrm{a} + \langle n_\mathrm{r}\rangle\epsilon_\mathrm{r}$ and $\epsilon_\mathrm{a} = -0.6$ kcal/mol and $\epsilon_\mathrm{r} = 1.2$ kcal/mol, as in our analysis of the desorption experiments (see section 5(ii)). At $T = 200$ K as in the experimental curve, $\langle n_\mathrm{a}\rangle$ and $\langle n_\mathrm{r}\rangle$ were calculated according to the procedure described in section 4(ii). The coordination numbers used are $Z_\mathrm{a} = 6$ and $Z_\mathrm{r} = 6$ as appropriate for an ideally organized CO adlayer. At high coverages when domain boundary effects become significant, the effective coordination number may be different. However, these effects are not expected to play an important role at the early and intermediate stages of the adsorption process. The value of a was set to $a = 0.077$, to ensure $S^* = 0.62$ as found experimentally. As in curves a and b, the values of S_1 and q used are 1 and 0.6, respectively.

It should be stressed that we do not interpret the good agreement between curve c and the experimental $S(\theta)$ in Figure 7 as supporting the suggested form of $S_0(\theta)$. Clearly, other parametrizations of $S_0(\theta)$ or other quantities in $S(\theta)$ could yield similarly good agreement. Our main goal here was to show that adsorbate lateral interactions might explain some of the features, for which common models (such as Kisliuk's or its variants) cannot account. In section (ii) that follows, we consider the effects of such interactions on the observed TPD spectra.

(*ii*) *Desorption Kinetics*. In order to calculate the TPD spectra, we solve analytically eq 7, 9, and 11 and then numerically integrate eq 12. In the theoretical analysis of the desorption process only, few parameters are involved and *all* but one are taken from the experimental data.

Recall that from the line-shape analysis of the α-peak in the TPD spectrum (Figure 1, section 3), we obtained $\nu \approx 10^{11}$ s^{-1} and $E_\alpha^0 = 23$ kcal/mol for the frequency factor and the desorption activation barrier (at $\theta_\alpha \rightarrow 0$), respectively. Also, the parameter b appearing in the empirical formula for the coverage-dependent activation energy used in the above analysis, $E_\alpha(\theta) = E_\alpha^0 + b\theta$ was found to be $b = 5$ kcal/mol. This has been obtained for low θ_α (=0.07), where according to our model the lateral interactions are primarily attractive. Specifically, at these low coverages, we can safely set $\langle n_\mathrm{r}\rangle = 0$ (i.e., no neighbors in repulsive NN positions). Thus, comparing eq 7 for $E_\alpha(\theta)$ with the empirical expression above, we find $b\theta_\alpha = \langle n_\mathrm{a}\rangle\epsilon_\mathrm{a}$ ($\theta_\alpha \ll 1$), and furthermore,

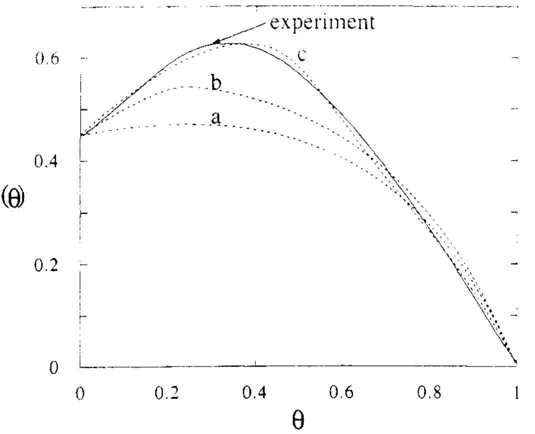

Figure 7. Experimental vs model theoretical results (curves a–c) for the total sticking probability as a function of CO coverage (see text). Experimental conditions as in Figure 4.

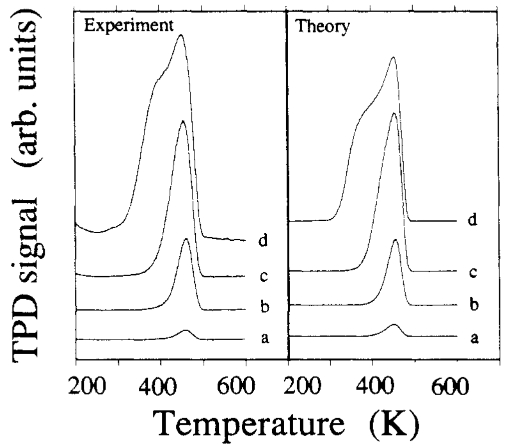

Figure 8. Experimental vs model theoretical results for the TPD line shape of the α-CO state, as a function of initial coverage: (a) $\theta_\alpha = 0.02$, (b) $\theta_\alpha = 0.15$, (c) $\theta_\alpha = 0.4$, (d) $\theta_\alpha = 0.75$.

from eq 9, we get $\langle n_a \rangle \simeq (Z_a + Z_r)\theta_\alpha$. For the hexagonal lattice, $Z_a + Z_r = 12$ and one gets $b \approx 12\epsilon_a$. Inserting the experimental value of $b = 5$ kcal/mol, we find $\epsilon_a \approx 0.4$ kcal/mol. As mentioned earlier, the size of a colony on the hexagonal lattice (as in a perfect Re(001) surface) is 12 sites, and the natural way to determine Z_a and Z_r is to assign all the NN sites as repulsive and all NNN sites as attractive, i.e., $Z_a = Z_r = 6$. This leaves us with only one unknown parameter, ϵ_r. We know that it should be repulsive and of the same order as ϵ_a; as a first (arbitrary) choice, we have used $\epsilon_r = -1$ kcal/mol. Integration of eq 12 with these parameters, with use of the experimental rate of the temperature sweep (B = 12.3 K/s), gives a fair reproduction of the TPD spectra.

A better fit to the experimental results can be obtained if we relax the requirement $Z_a = Z_r$ and set instead $Z_r > Z_a$. While this assumption may, at first sight, appear rather arbitrary, there is in fact a very good reason to assume that at high coverages the effective number of attractive next-nearest-neighbors is in fact less than $Z_a = 6$. As discussed in section 4, in the CO/Re, many small α-CO domains with molecules located at favorable NNN positions start forming around the β nucleation centers. Most of these domains are not in register with each other, thus giving rise to antiphase grain boundaries as coverage increases. As a consequence, in a colony located at the vicinity of such a grain boundary, some of the NNN sites, which in a perfectly ordered phase would have an attractive character, are now partly or completely excluded due to the repulsion from the neighboring phase, as illustrated in Figure 6. Since in our system there are many different α-CO domains, this "grain boundary effect" is significant and effectively reduces Z_a. Similar effects of adsorbate repulsions at grain boundaries on adsorption kinetics and TPD spectra have been inferred by other authors.[7,13]

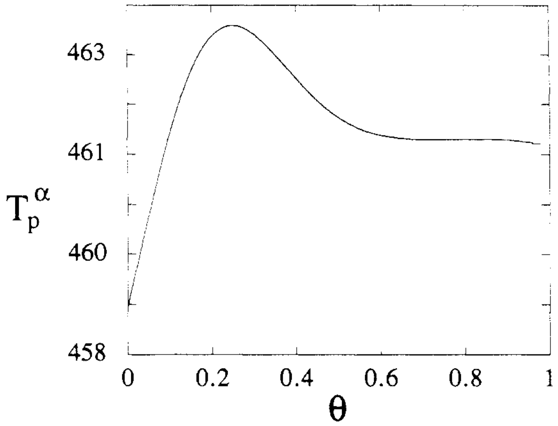

Figure 9. Model theoretical results for the variation of the α-CO peak desorption temperature with initial α-site coverage.

Integration of eq 12 with $Z_a = 3$ and $Z_r = 6$ (using $\epsilon_a = 0.6$ kcal/mol, $\epsilon_r = -1.2$ kcal/mol) yields the TPD spectra shown in Figure 8, which are in excellent agreement with the experimental spectra. The resulting theoretical peak temperature, T_p^α, is shown in Figure 9 as a function of initial coverage. The qualitative similarity to the experimental curve, Figure 5, is apparent. However, the range of variation of T_p^α is considerably smaller than the experimental one.

6. Summary and Conclusions

The adsorption–desorption kinetics of CO molecules on a Re(001) single-crystal surface have been studied experimentally and theoretically for different coverages and crystal temperatures in the range 80–360 K. The two distinct CO adsorption sites, α and β, were found to be coupled in a way that generates a nonstandard coverage dependence of the sticking probability, with $S(\theta)$ reaching a maximum at an intermediate coverage of $\theta \approx 0.35$. The peak desorption temperature of the α-CO state, T_p^α, was found to increase from 440 K near zero α-CO coverage to 465 K at $\theta_\alpha \approx 0.1$ (i.e., $\theta \approx 0.3$) and then decrease to ~455 K at saturation coverage. The experimentally obtained initial sticking probability of CO on Re(001) ($S_0 = 0.45$) is about half of the common value observed for CO on other metals. The uncertainty in the number of adsorption sites (N_s) at saturation coverage, which is due to the absence of an ordered structure at any coverage, may lead to higher (or lower) values of S_0. The physical reason for this small value of S_0 is currently unknown and deserves further investigation.

Our theoretical model for the kinetics of adsorption is based upon regarding the β-sites as traps for diffusing α-CO and gas-phase molecules. The chemisorbed molecules enhance further adsorption by serving as "antenna" for capturing gas-phase molecules. This picture explains the important qualitative features of the rather unusual coverage-dependent sticking probabilities. Nearly quantitative agreement can be achieved by a proper choice of parameters. Yet, it should be stressed that other choices of parameters or somewhat different models could possibly lead to similar results.

The experimental desorption characteristics reflected by the TPD spectra have been accounted for based on a simple statistical mechanical model. A lattice gas-type model that takes into account both repulsive (nearest-neighbor) and attractive (next-nearest-neighbor) interactions among the adspecies, provides an adequate reproduction of the desorption spectra. This includes the variation of T_p^α with coverage and, moreover, the details of the TPD line shapes. In particular, the model predicts the appearance of a low-temperature shoulder in the α TPD peak at high coverages. It should be stressed that this feature is solely due to (repulsive) lateral interactions and is not, as is often suggested (including for the CO/Re system[17b]), due to population of different adsorption sites. Additional support for our interpretation is provided by high-resolution electron energy loss measurements,

J. Phys. Chem. **1989,** *93,* 8067–8072

revealing a single loss feature (hence adsorption site) at all coverages.[17a]

Acknowledgment. This research was supported by a grant from the Israeli National Council for Research and Development and the VDI, Düsseldorf, Germany. The Fritz Haber Research Center is supported by the Minerva Gesellschaft fur die Forschung mbH, Munich, BRD.

Registry No. CO, 630-08-0; Re, 7440-15-5.

Eutectic Mixtures of Ferroelectric Liquid Crystals

J. W. Goodby,*

School of Chemistry, The University, Hull, HU6 7RX, England

E. Chin,

AT&T Bell Laboratories, Murray Hill, New Jersey 07974

and J. S. Patel

Bellcore, Redbank, New Jersey 07701 *(Received: February 6, 1989)*

Ferroelectric liquid crystals show potential as the optically and electrically active media in a variety of applications. However, it is considered unlikely that a single individual compound will possess all of the desired properties required by device applications, and therefore it is to be expected that it will be necessary to mix compounds together in order to obtain a suitable blend. In this study we have examined how the pitch of the helix and the magnitude of the spontaneous polarization of the ferroelectric smectic C* phase vary as a function of concentration when two materials of opposite twist and with the same (or opposite) polarization directions are mixed together. In some cases the ferroelectric phase(s) was found to disappear in the central region of the phase diagram, only to be replaced by the nonferroelectric smectic B phase. This type of behavior was found to happen even when the two components were of the same generic family. Changes in phase type were detected optically and also from the switching behavior in individual mixtures. This second approach offers a new method of monitoring certain phase changes that occur in a phase diagram.

Introduction

The use of multicomponent phase diagrams in liquid crystal systems is of historical importance in both the identification of mesomorphic phases[1-3] and the generation of commercial mixtures for display devices.[4] Consequently, phase diagrams are used extensively in the investigation of chemical and physical interactions that occur between components in mixtures. In this article we examine some of the effects obtained in binary mixtures when various ferroelectric liquid crystals, which have different physical properties, are mixed together. Ferroelectric liquid crystals are particularly good candidates for probing intermolecular interactions in smectic phases because they possess a wide variety of physical properties that can be readily accessed by simple experimental techniques. The chiral smectic C* phase has a layered structure where the elongated molecules are packed in a tilted orientation with respect to the layer planes. On passing from layer to layer there is a precession of the tilt direction of the molecules, thereby forming a macroscopic helix. The helix can either twist to the left or right depending on the spatial configuration(s) of the molecules. The pitch of the helix so formed is dependent on the degree of chirality and the optical purity of the constituent materials. Essentially, each individual layer of molecules has a "local" C_2 symmetry axis which lies parallel to the plane of the layers, and in a direction normal to the vertical planes that contain the long axes of molecules. It is along this axis that the spontaneous polarization is manifested.[5,6] Consequently, because the layer has an "environmental" twofold symmetry axis, the spontaneous polarization can develop in either direction along it, thereby giving a direction to the polarization [Ps(+) or Ps(−)], i.e., the polarization is a vector quantity.[7] In the bulk phase the local polarization, with respect to each layer, is rotated about an axis normal to the layers on moving from one layer to the next. Thus, the net polarization of the bulk phase, even though the local C_2 symmetry is retained, is reduced to zero.[8] However, if the helix is compensated then the bulk phase becomes ferroelectric. The structure of this phase is such that the tilted orientation of the molecules and the direction of the polarization within each layer are coupled. This means that the director and the direction of the macroscopic spontaneous polarization of the bulk system are also coupled to each other. Thus, in a material with a large pitch, the optic axis and the polarization are coupled. Such a relationship can be exploited in electrooptic modulators.

Four properties of ferroelectric liquid crystals that are relevant in the above context are the twist sense, pitch, polarization direction, and the magnitude of the polarization. All of these properties can be controlled and investigated to some extent in mixtures. For practical purposes, it is usually desirable to increase the pitch of the phase while at the same time maintaining a reasonable polarization.[9] The pitch of a ferroelectric phase can be increased for a given material by mixing it with another compound of opposite twist sense.[10] In such a binary mixture the two helical structures compensate for one another, and thus the pitch of the mixture is usually greater than that of either component in the binary mixture. At a certain concentration, the two twists will be completely compensated and the pitch will become infinite. At this point the value for the polarization need not become zero because this will depend on whether or not the two materials have similar polarization values and the same polarization directions. Thus, it is possible to find a point in the phase diagram where the pitch becomes infinite but the polari-

---

(1) Sackmann, H.; Demus, D. *Mol. Cryst. Liq. Cryst.* **1966,** *2,* 81.

(2) Goodby, J. W. *Mol. Cryst. Liq. Cryst. Lett.* **1983,** *92,* 171.

(3) Demus, D.; Goodby, J. W.; Gray, G. W.; Sackmann, H. *Mol. Cryst. Liq. Cryst. Lett.* **1980,** *56,* 311.

(4) Demus, D. In *Nonemissive Electrooptic Displays*; Kmetz, A. R., von Willisen, F. K., Eds.; Plenum: New York, 1976; pp 83–119.

(5) Meyer, R. B.; Liebert, L.; Strzelecki, L.; Keller, P. *J. Phys. (Paris) Lett.* **1975,** *36,* L69.

(6) Meyer, R. B. *Mol. Cryst. Liq. Cryst.* **1976,** *40,* 74.

(7) Clark, N. A.; Lagerwall, S. T. *Ferroelectrics* **1984,** *59,* 121.

(8) Brand, H. R.; Cladis, P. E.; Finn, P. L. *Phys. Rev.* **1985,** *31A,* 361.

(9) Patel, J. S.; Goodby, J. W. *Opt. Eng.* **1987,** *26,* 373.

(10) Gray, G. W.; McDonnell, D. G. *Mol. Cryst. Liq. Cryst. Lett.* **1977** *34,* 211.

0022-3654/89/2093-8067$01.50/0